JoT JOURNAL OF TURBULENCE

http://jot.iop.org/

Synthetic jet control for flows in a diffuser: vectoring, spreading and mixing enhancement

Maher Ben Chiekh[1], Jean-Christophe Béra[2] and Michel Sunyach[2]

[1] Laboratoire d'étude des systèmes thermiques et énergétiques, Ecole Nationale d'Ingénieurs de Monastir, Monastir 5019, Tunisia
[2] Laboratoire de mécanique des fluides et d'acoustique, Ecole Centrale de Lyon, 69134 Ecully Cedex, France
E-mail: Maher.benchiekh@enim.rnu.tn

Received 15 May 2003
Published 11 December 2003

Abstract. This experimental study examines the efficiency of wall pulsing control that is applied to a confined flow going through a two-dimensional diffuser continued by a duct. One- and dual-side pulsing generated by synthetic jet actuators are tested as control means. Particle image velocimetry is used to investigate instantaneous velocity fields and obtain quantitative information. One-side pulsing provokes vectoring of the primary flow in the same direction as the periodic excitation and increases its lateral expansion. Dual-side pulsing neutralizes vectoring but is more efficient for spreading. In both cases, the inner structure of the primary flow was found to be strongly modified, with the generation of highly periodic large-scale structures which kept the flow attached to the diffuser walls. The fluctuating velocity maps point out that the high-fluctuation zone greatly spreads out under control. The flow is considerably widened and the mixing is enhanced.

PACS numbers: 47.27.Wg, 47.60.+i

JoT 4 (2003) 032

 PII: S1468-5248(03)63604-0 1468-5248/03/000001+12$30.00

Contents

1. Introduction

1.1. Fluid control in diffusers

In internal flow systems, it is often necessary to decelerate the fluid, i.e. to pass the flow through a diffuser. It plays an important role in many mechanical systems, such as vehicles' motors, hydraulic channels and compressors. The main function of the diffuser is to convert the dynamic pressure into static pressure. An ideal diffuser is one that gives a steady and symmetric flow at the exit and a maximum pressure recovery. Experiments indicate that maximum performance is obtained only when the diverging half-angle is less than 7°. However, in order to save space, constructors are often forced to employ short and subsequently wide-angle diffusers. These diffusers often suffer from severe deficiencies, low performance, flow asymmetry at the exit and large unsteady pressure fluctuations.

It has been recently recognized that flow control constitutes an efficient way to modify flow separation from bodies. Different devices for separation control have been reported by Gad-el-Hak *et al* [1]. In the case of diffusers, extensive experimental results have been reported by MacManus and Magill [2]. Pulsed blowing jets were placed close to the diffuser inlet to generate a high vorticity zone, which was largely responsible for the intense mixing achieved at the diffuser inlet. Through this mixing action, the separation of the boundary layer may be delayed or even suppressed. Kwong and Dowling [3] used small-amplitude blowing and suction from the diffuser lip. They found that the control reduces the energy losses and attenuates the unsteadiness generated by the boundary layer separation.

In the present investigation, synthetic jet control is used. This control technique has shown a high efficiency in aerodynamics. The diffuser was designed such that injection could be introduced in the streamwise direction. Previous results obtained with cross-stream injection can be found in [4].

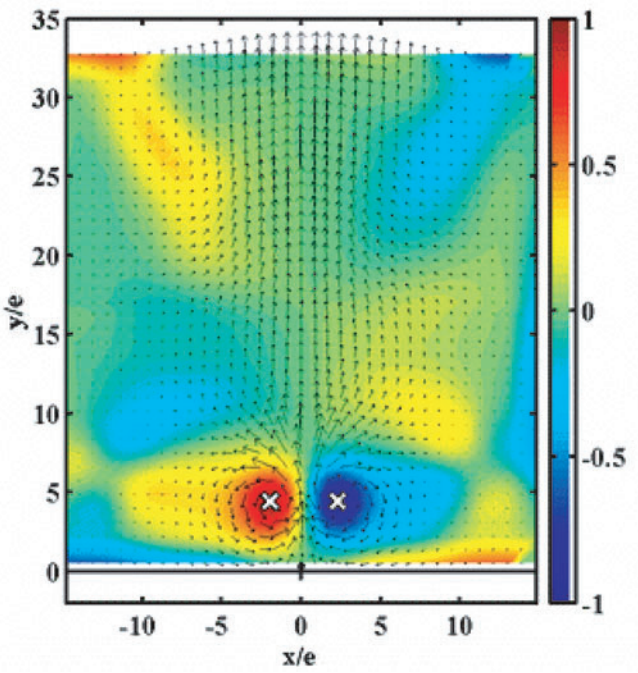

Figure 1. Phase-averaged velocity field combined with the eddy structure identification algorithms from the experiments of Béra *et al* [6] (see animation).

1.2. Synthetic jet

The synthetic jet (i.e. a zero-net-mass-flux injection made of alternate blowing and suction) has been the focus of significant experimental research activity [5–7]. Furthermore, several computational studies described the fundamental aspects of the generated flow [8, 9]. From these works, the synthetic jet has emerged as a very promising control technique for many applications such as thrust vectoring of jet engines [10], mixing enhancement [11, 12] and control of separation [13, 14].

A typical synthetic jet actuator uses a vibrating diaphragm to drive oscillating flow through a small orifice or slot. The common design represents an electromechanical–acoustic coupled system with adjustable amplitudes and frequencies. A full study of synthetic jet devices can be found in [7]. Although there is no mean injection of mass, the authors conclude that in the far field, a synthetic jet bears much resemblance to a continuous jet. However, in the near field, a synthetic jet is dominated by vortex pairs that entrain more fluid, and thus grows more rapidly than a continuous jet.

The particle image velocimetry (PIV) investigation of the synthetic jet realized by Béra *et al* [6] has shown that well-organized flow patterns dominate the velocity fields by periodic flux of contra-rotating eddy pairs. There is a corresponding large lateral expansion of the jet and a large entrainment rate of external fluid, compared to usual steady jets. This property is basically linked to the self-induced convective motion of eddy pairs. The flow structures may vary significantly from one injection cycle to another, but phase-average eddies are well identified and can be traced over the whole injection cycle, as illustrated in figure 1.

The aim of the present study is to describe the interaction between synthetic-jet pulsing and a diverging flow. The paper is organized as follows. The experimental set-up with the actuator characteristics and the PIV system are described in section 2. Results dealing with the velocity

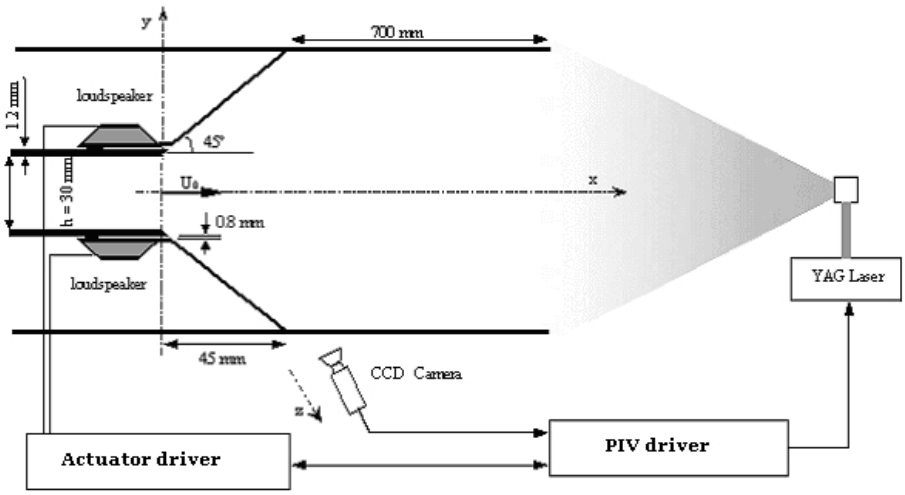

Figure 2. Schematic of the experimental set-up.

fields, streamline patterns and kinetic energy maps are given and discussed in section 3. The flow control mechanism is presented in section 4.

2. Experimental set-up

2.1. Wind tunnel facility

Experiments were performed in a subsonic wind tunnel with a constant span of 0.12 m. A schematic diagram of the tunnel is shown in figure 2. The blow down the tunnel is driven by a centrifugal fan. The flow passes through a plenum section with screens and honeycomb and through a progressive 4 : 1 contraction to reduce turbulence and improve flow uniformity. The air exits from a short rectangular tube (height: $h = 3$ cm, span $4h$ and length $13h$). The velocity of the out-going flow was $U_0 = 18\,\mathrm{m\,s^{-1}}$. This gives a jet Reynolds number equal to 36 000. A symmetrical two-dimensional (2D) diffuser (angle, $2 \times 45°$; area ratio, 4 and outlet height, 12 cm) is placed at the flow exit. The diffuser then opens on to a 70-cm-long confined duct. Perspex walls were used to provide optical access. For all subsequent graphical illustrations, the origin is located at the diffuser entrance, at the intersection of the vertical and horizontal planes of symmetry.

2.2. Synthetic jet actuator

A pair of pulsed injection actuators is positioned at the lip of the diffuser. The actuators are similar to the electro-dynamical 'synthetic jet' generators described in detail by Béra *et al* [6]. The actuator slit dimensions were $e = 0.8$ mm width and 95 mm span. Each slit was fed by a pulsed cavity having the wall upstream of the diffuser as cover. Pressure fluctuations in the cavity were generated by a loudspeaker fed by a sinusoidal electric current.

The driving frequency in the present experiment was 100 Hz. Hot-wire anemometer measurements show that the interaction between the synthetic jet actuator and the primary flow is the largest at this frequency, providing sinusoidal velocity signal at the slit exit with amplitude U_c equal to $32\,\mathrm{m\,s^{-1}}$. The Strouhal number $St = 0.17$, a value close to the result found by the numerical predictions ($St = 0.20$) of Freund and Moin [15] for the most efficient

spreading of jet flow. This velocity corresponds to a mass rate ratio between the actuator response and the primary flow of

$$\frac{\dot{M}_{\text{blowing}}}{\dot{M}_{\text{jet}}} = \frac{2e_c U_c/\pi}{hU_0} = 0.030 \text{ per unit span.} \quad (1)$$

This value is of the same order as that used by Freund and Moin (0.035).

Under these conditions, three configurations of control were tested: (i) upper-side control with upper actuator on, (ii) lower-side control with lower actuator on and (iii) dual control with upper and lower actuators working in phase.

2.3. Velocity measurement and post-processing

All velocity measurements were performed using the PIV technique. The flow was seeded with small oil droplets of approximately 1–2 μm diameter, produced by a smog generator located at the inlet of the wind tunnel fan. Measurements were carried out with a Dantec system using two coupled YAG laser sources (300 mJ Quantel lasers). The time delay between two pulses was 15 μs. Each laser was operated in a single Q-switch mode and signals generated by the synchronization module inside the PIV processor control the firing of the laser cavities and hence the interval between pulses. The laser output was shaped into a light sheet and directed through the test section by using fibre optics. The thickness of the light sheet at the measurement section was 1 mm. The light scattered by the seeding particles was recorded from the side with a 1280×1018 pixels Kodak Megaplus ES-1-0 CCD camera. Pairs of raw images, acquired at 2.2 Hz, were cross-correlated by using 32×32 pixel interrogation windows, with a 50% overlap ratio between adjacent windows. The resulting spatial resolution of the PIV measurement was 1.9×1.9 mm.

To study the evolution of these structures during a cycle, the image acquisition was locked in-phase with the pulsing control signal. Hence, an external timer was used to trigger the actuators and the PIV system at the same time. A time delay was applied on the PIV triggering in order to acquire images at different instants of the pulsing cycle. The time delay could vary to sweep the whole cycle. The phase-average velocity field at every 20° step could therefore be recorded for all types of control. Post-processing measurements were obtained by the combination of conventional statistical tools and algorithms based on the work of Graftieaux *et al* [16].

3. Mean flow results

3.1. Characterization of the flow without control

The mean velocity field is presented in figures 3(a) and (b). In the absence of any flow control, the flow through the wide-angle diffuser consists of a typical confined jet having two states of stability: one observes a deviation of the jet either towards the upper wall or towards the lower wall. This is due to the need for the flow to join the wall, known as the Coanda effect. The jet is surrounded by regions of separated flow.

The map of fluctuating kinetic energy $\bar{k} = 1/2(\overline{u'^2} + \overline{v'^2})$ when the flow is deviated towards the lower wall is shown in figure 3(c). One can observe the shear zone that limits the flow, the maximal values registered correspond to $\sqrt{\bar{k}}/U_0 = 0.20$. The streamlines shown in figure 3(d) indicate the formation of a large vortex in the region limited by the primary flow and the lower wall. On the opposite side, there is a secondary incoming flow downstream from the upper wall, up to the diffuser, before changing direction and joining the primary flow: this flow is responsible of the primary flow entrainment. Streamline patterns permit to estimate the position of the reattachment of the flow on the lower horizontal wall at $x/h \approx 6$.

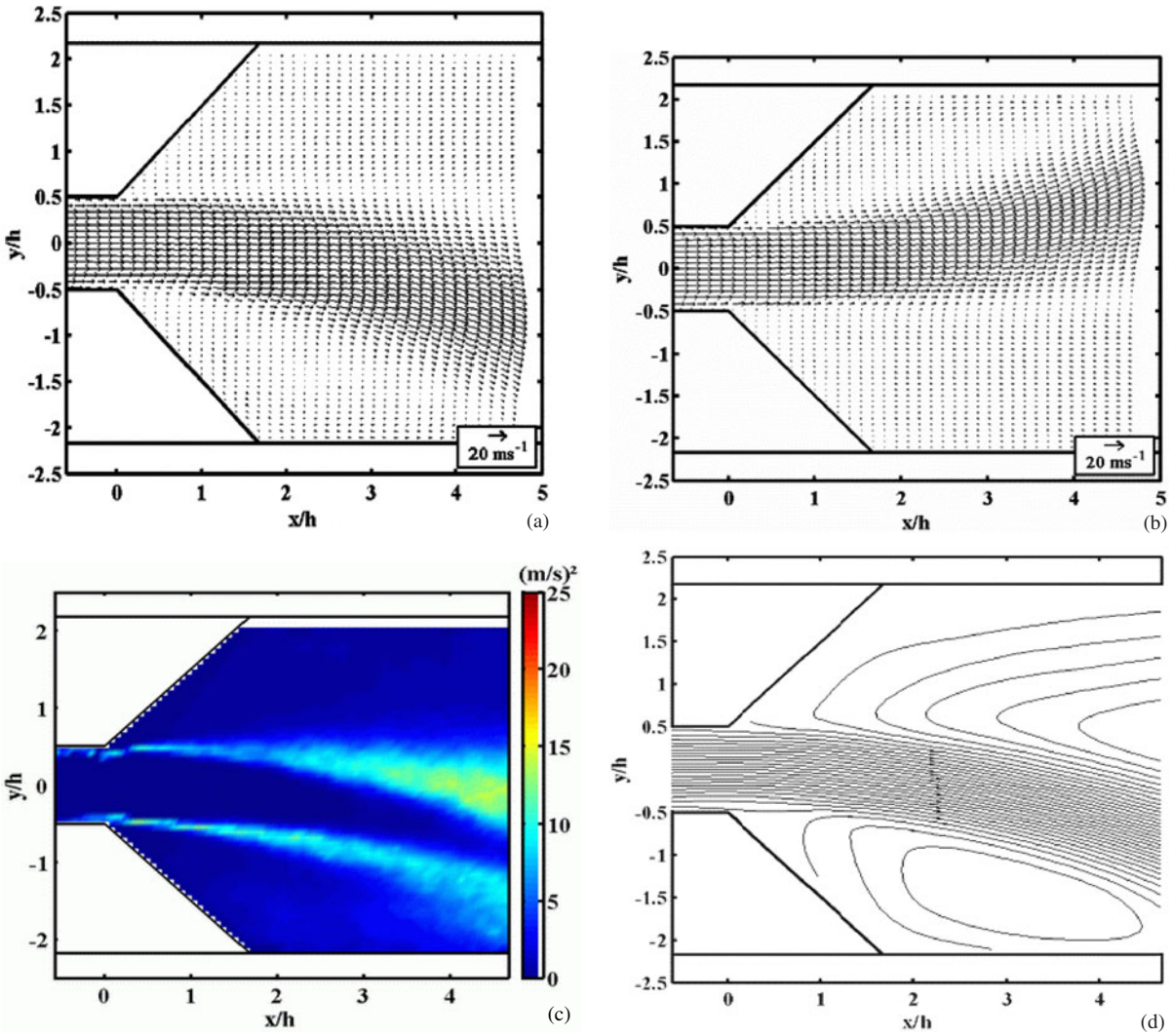

Figure 3. Characterization of the flow without control. (a) Mean velocity field: lower-side stability state; (b) mean velocity field: upper-side stability state; (c) map of fluctuating kinetic energy for lower-side stability state; and (d) streamline patterns for lower-side stability state.

3.2. Effects of one-side control

Figure 4 illustrates the mean velocity fields, fluctuating kinetic energy and streamline patterns for the one-side control at 100 Hz. The case of lower-side control has been chosen. One observes a deviation of the flow towards the controlled side and an important widening of the flow. These spreading and vectoring are associated with the entrainment of the surrounding fluid: in particular, as indicated by streamlines of figure 4(c), a reverse flow along the upper diffuser wall is visible and feeds the enlarging flow. The deviation is significant and reaches more than 20° downwards for lower-side control. The spreading rate increase has been estimated to be 40%. It is also important to note that if before control the primary flow was in its upper stable position then a lower-side control imposes its rules. Finally, the reattachment of the flow to the horizontal wall occurs at $x/h \approx 4$, whereas without control this distance was around $x/h \approx 6$.

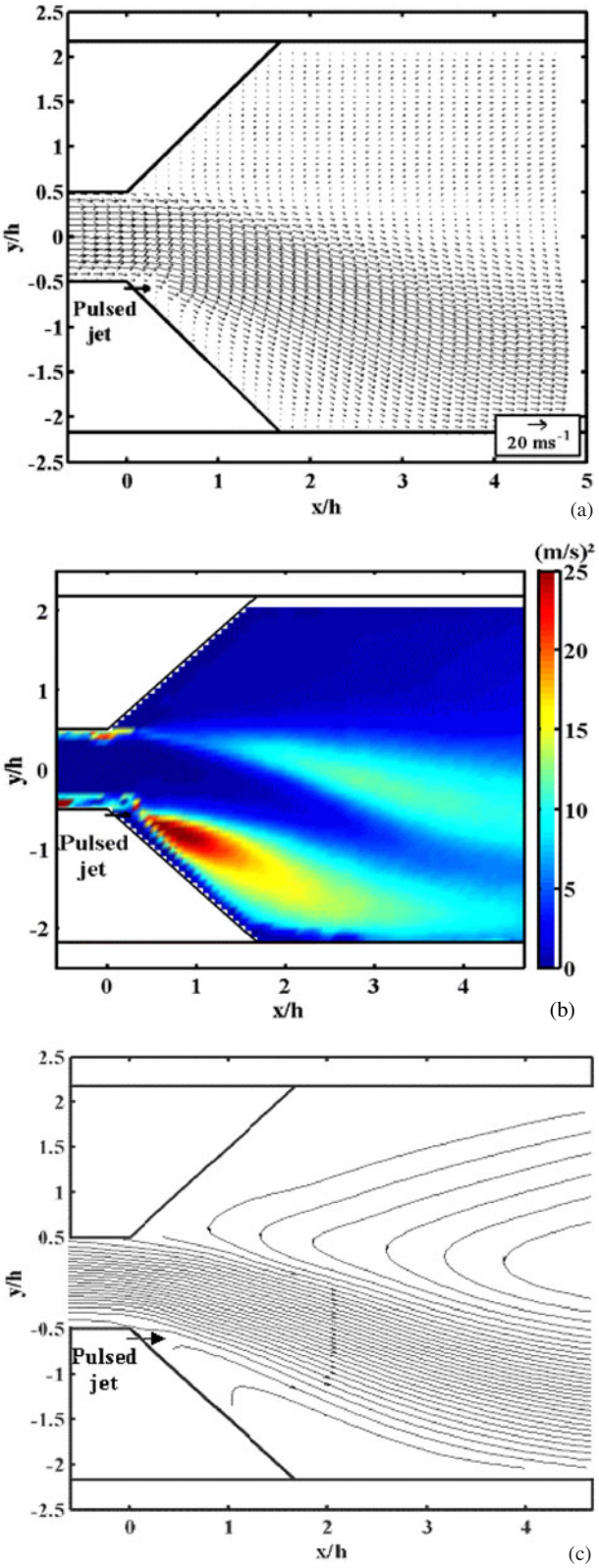

Figure 4. Characterization of the flow under lower-side control: (a) mean velocity field; (b) map of fluctuating kinetic energy; and (c) streamline patterns.

The maps of fluctuating kinetic energy are plotted in figure 4(b). When compared with figure 3(c), the following three results can be summarized:

(i) The fluctuation intensity is increased by the control: $\sqrt{\overline{k}}/U_0$ reaches 0.30 compared with the value 0.20 without control.

(ii) The wall pulsing generates a large area of strong fluctuations in the vicinity of the controlled side of the diffuser; without control, a strip of high fluctuations is attached to each one of the shear layers of the flow jet.

(iii) The area of intense fluctuations lies in front of the actuator and spreads significantly downstream, with a maximum intensity around $x \approx h$; the maximum intensity without control is weaker than with control and it occurs around $x \approx 4h$.

3.3. Effects of dual-side control

Figures 5(a)–(c) illustrate the results when both actuators are operating. The dual-side control clearly neutralizes the vectoring and gives the flow a median position because the two actuators pull the fluid in opposite directions. Most important is that the dual side provides an additional increase in the spreading rate by around 20% compared to the rate obtained by one-side control. Thus, the total spreading rate increase reaches 60%.

The maps of fluctuating kinetic energy, plotted in figure 5(b), show two intense fluctuating zones, one on each side of the diffuser. Compared to one-side control, the location of each fluctuating area is now further away from the wall and their intensity is approximately the same. The inner structure of the jet flow is strongly modified; in particular, the potential cone length is reduced considerably. The two shear layers interact very early, at $x \approx 2h$, against $x \approx 4h$ for one-side control and $x \approx 6h$ for natural flow.

Streamline patterns presented in figure 5(c) show that the reattachment of the primary flow, observed in the lower-side control at $x/h \approx 4$ and around $x/h \approx 6$ without control, was pushed back under the dual-side control.

3.4. Comparison of the different control configurations

Figure 6 summarizes the main results obtained for all control configurations by presenting mean velocity profiles at the diffuser exit: existence of two stability states for the uncontrolled flow, vectoring and entrainment under one-side control, and substantial flow expansion under dual-side control. It can be observed that the impact of the upper- and lower-side controls is not perfectly symmetrical: the upper-side pulsing deviates the jet a little more but enlarges it a little less than the lower-side pulsing. In the same way, the dual-side controlled flow is not exactly centred on the incoming flow centreline, but deviates slightly upwards, indicating that the upper-side pulsing would be more efficient than the lower-side pulsing. This asymmetry between upper- and lower-side control is probably due to a very slight manufacturing difference between both actuators. It shows the high sensitivity of the flow to the asymmetry of the control.

4. Control mechanism

Figures 7(a) and (b) depict animations of phase-averaged velocity fields combined with the eddy-centre criterion at different pulsing phases for the lower- and dual-side controls, respectively. The phase numbers correspond to the phase of the electrical input signal for the actuator excitation. Hot-wire measurements show a phase shift of nearly 50° between the input and the output

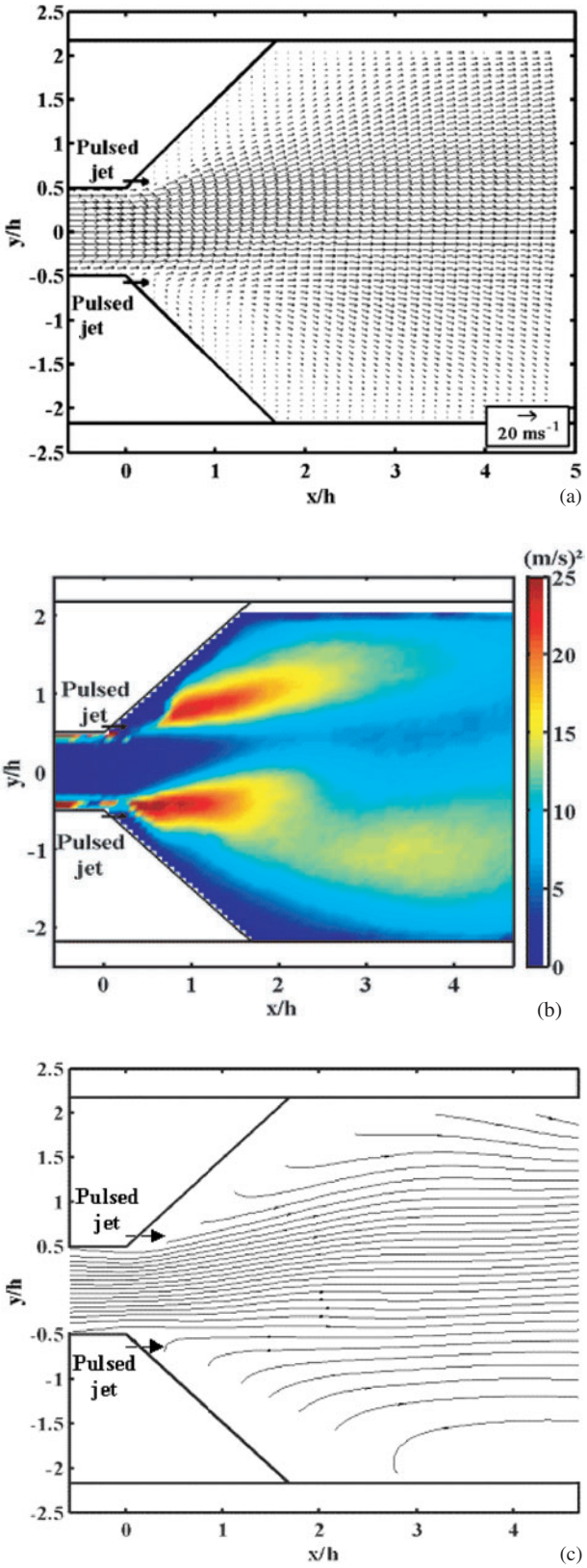

Figure 5. Characterization of the flow under dual-side control: (a) mean velocity field; (b) map of fluctuating kinetic energy; and (c) streamline patterns.

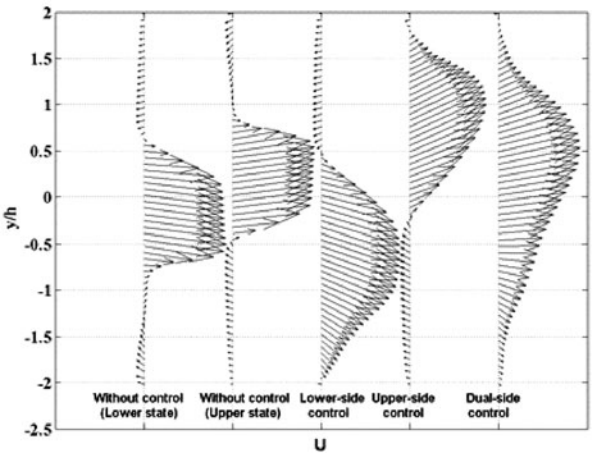

Figure 6. Mean velocity profile at the diffuser exit for all situations.

actuator signals. Large-scale flow structures, whose centres are marked by a cross symbol (x), are generated by the wall pulsing. These structures are localizable on each phase average of the velocity fields, bringing some physical insight into the control mechanism. In particular, the averaged eddies generated by the control can be followed over the pulsation cycle, showing their progressive convection. The distance of approximately $2.5h$ between the successive eddies corresponds to the eddy displacement during one cycle. Thus, in every case of control, the convection velocity can be estimated at $0.42U_0$, which is in the usual range of values for eddy convection velocity in a separated layer.

Figure 7(c) illustrates the average-phase location of eddy structures over one period of the jet pulsing for one- and dual-side controls. The mean location is marked by open circles. For one-side pulsing, a contra-rotating structure appears on the uncontrolled side. This structure is roughly symmetrical to the active structure created by the control, with respect to the axis of the deviated jet. Physically, it is linked to the unsteady entrainment on the uncontrolled side. For the dual-side control, the results clearly show the symmetrical generation and convection of the control structures.

The instantaneous eddy locations can largely differ from the phase-average position. Their centres can be obtained by the eddy-centre criterion on each instantaneous field. Thus, the scatter can be estimated at each phase of the controlled jets. For example, figure 7(d) presents the eddy centres at a phase corresponding to the beginning of the suction. In this case, the scatter is small, showing that the eddy structures remain periodic. When convected out of the diffuser, periodicity is progressively lost. The structure is then blurred in the averaging process.

In conclusion, the control mechanism is based on a periodic generation of eddies near the diffuser wall. On one side of these eddies, their flux is part of the primary flow, and on the other side, they roll along the diffuser wall. These structures force the primary flow to come closer to the diffuser wall.

5. Main results

Wall-pulsed injection is an interesting way to modify the flow in a diffuser. In the present work, synthetic jet technology was used to control the flow in a short wide-angle diffuser. The flow dynamics was analysed from particle image velocimetry measurements.

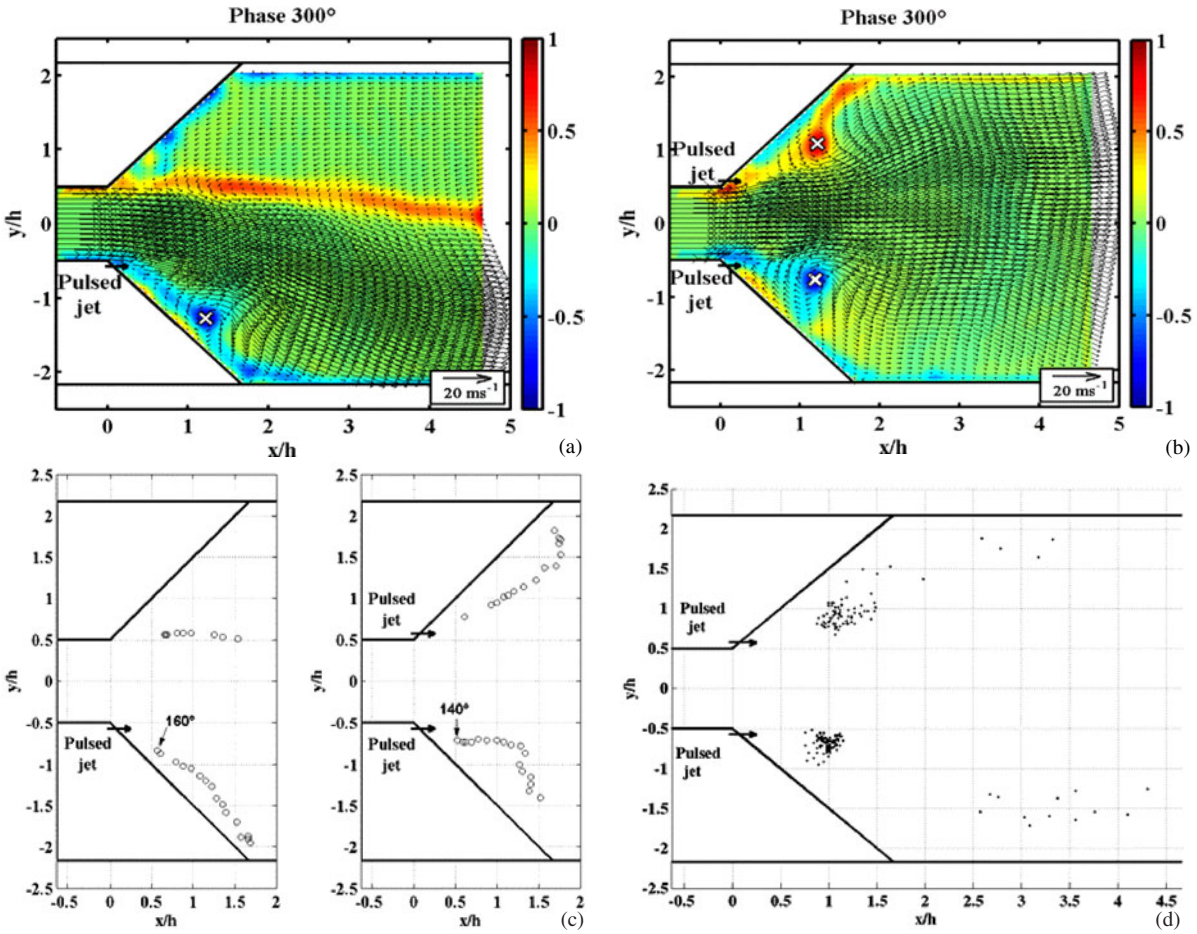

Figure 7. (a) Phase-averaged velocity combined to eddy structures criteria with lower-side control (see animation). (b) Averaged velocity combined to eddy structures criteria with dual-side control (see animation). (c) Locations of mean eddy structures on one period of wall pulsing: lower-side pulsing (left); dual-side pulsing (right). (d) Instantaneous positions of eddy centres recorded at a same phase of control at the beginning of the sucking phase of the lower actuator.

The mean velocity fields without control reveal a bistable flow. The boundary layer separation caused by reverse flow is provoked at the diffuser inlet. With a lower-side pulsing jet, the reverse flow intensity is reduced and the primary flow is entrained towards the active wall. A high-vorticity zone is developed at the diffuser entrance, which enhances mixing and delays boundary layer separation. The flow section is increased by 40%. The flow deflection reaches more than 20° at the diffuser exit. The dual-side pulsing centres the primary flow such that it neutralizes vectoring, but it provides an important mixing enhancement and enlarges the flow section. The flow spread increase reaches more than 60%.

The analysis of the synchronized velocity fields permits the tracking of the flow evolution along the injection cycle. These fields indicate the presence of an eddy structure generated during the blowing phase of the synthetic jet. The analysis of the dynamics of this eddy structure and its interaction with the primary jet reveal the importance of both the blowing and the suction phases for the control mechanism.

Acknowledgements

The authors gratefully acknowledge numerous important contributions by G Comte-Bellot, M Michard and N Grosjean during the course of the work and the preparation of the manuscript. This work was supported by Rhône-Alpes MIRA program for French–Tunisian collaboration.

References

[1] Gad-el-Hak M, Pollard A and Bonnet J P 1998 *Flow Control: Fundamentals and Practices* (Berlin: Springer)
[2] MacManus K and Magill J 1997 Airfoil performance enhancement using pulsed jet separation control *Proc. 4th AIAA Conf. Shear Flow Control* (Snowmass Village, CO, USA) AIAA Paper 97-1971
[3] Kwong A H M and Dowling A P 1994 Active boundary-layer control in diffuser *AIAA J.* **32** 2409–14
[4] Ben Chiekh M, Béra J C, Michard M and Sunyach M 2000 Contrôle par jet pulsé de l'écoulement dans un divergent court à grand angle—(pulsed jet control of a short divergent) *C. R. Acad. Sci. Paris* **328** (Sér. II.b) 749–56
[5] Smith B L and Glezer A 1998 Jet vectoring using synthetic jet actuators. The formation and evolution of synthetic jets *Phys. Fluids* **10** 2281–97
[6] Béra J C, Michard M, Grosjean N and Comte-Bellot G 2001 Flow analysis of 2D pulsed jets by particle image velocimetry *Exp. Fluids* **30** 519–32
[7] Glezer A and Amitay M 2002 Synthetic jets *Annu. Rev. Fluid Mech.* **34** 503–29
[8] Kral L D, Donovan J F, Cain A B and Cary A W 1997 Numerical simulation of synthetic jet actuators *Proc. 4th AIAA Conf. Shear Flow Control* (Snowmass Village, CO, USA) AIAA Paper 97-1824
[9] Mittal R and Rampunggoon 2001 Interaction of synthetic jet with flat plate boundary layer *Proc. 31st AIAA Conf. Fluid Dynamics & Exhibit* (Anaheim, CA, USA) AIAA Paper 2001-2773
[10] Smith B L and Glezer A 1997 Vectoring and small-scale motions effected in free shear flows using synthetic jet actuators *35th AIAA Aerospace Sciences Meeting* (Reno, NV, USA) AIAA Paper 97-0213
[11] Parekh D E, Kibens V, Glezer A, Wiltse J M and Smith D M 1996 Innovative jet control: mixing enhancement experiments *34th Aerospace Science Meeting* (Reno, NV, USA) AIAA Paper 96-0308
[12] Pack L G and Seifert A 1999 Periodic excitation for jet vectoring and enhanced spreading *37th AIAA Aerospace Sciences Meeting* (Reno, NV, USA) AIAA Paper 99-0672
[13] Amitay M, Smith B L, Kibens V, Parekh D E and Glezer A 2001 Aerodynamic flow control over an unconventional airfoil using synthetic jet actuators *AIAA J.* **39** 361–70
[14] Béra J C, Michard M, Sunyach M and Comte-Bellot G 2000 Changing lift and drag by jet oscillation: experiments on a circular cylinder with turbulent separation *Eur. J. Mech.* B **19** 575–95
[15] Freund J B and Moin P P 2000 Jet mixing enhancement by high-amplitude fluidic actuation *AIAA J.* **38** 1863–70
[16] Graftiaeux L, Michard M and Grosjean N 2001 Combining PIV, POD and vortex identification algorithms for the study of unsteady turbulent swirling flows *Measurement Sci. Technol.* **12** 1422–9